2021

R1234ze(E) As Drop-In Replacement For R134a In A Micro-Fin Shell-And-Tube Evaporator: Experimental Tests And Calculation Model

Giuseppe Censi
Onda S.p.A., Italy, gcensi@onda-it.com

Andrea Padovan

R1234ze(E) As Drop-In Replacement For R134a In A Micro-Fin Shell-And-Tube Evaporator: Experimental Tests And Calculation Model

Giuseppe CENSI*, Andrea PADOVAN

Onda S.p.A., R&D Department,
Lonigo, VI, Italy
Phone: +39 0444720720, Fax: +39 0444720721,
E-mail: gcensi@onda-it.com

* Corresponding Author

ABSTRACT

For the planned phase-down of the hydrofluorocarbon (HFC) R134a in vapor compression cycles, a reasonable and accepted long-term substitute is the hydrofluoro-olefin (HFO) R1234ze(E): due to similar operating pressures of the two fluids, an existing plant can be easily adapted to work with R1234ze(E) as a drop-in replacement for R134a.
This works presents a direct comparison of the experimental and calculated performances obtained by using R134a and R1234ze(E) in the same water-cooled chiller at the same operating conditions, focusing on the evaporator, a direct expansion shell-and-tube heat exchanger with micro-fin copper tubes.
The working conditions are set to typical air conditioning values: the evaporating temperature of the refrigerant ranges from 3.5 to 5.0 °C, and the outlet water temperature is kept at a constant value of 7 °C. As the refrigerant flows inside the tubes with one passage only, the mass flux values are quite low, ranging from 30 to 100 kg m^{-2} s^{-1}, with a constant inlet quality of 0.25 and an outlet superheating of 5 K. The average heat flux (referred to the whole heat exchanger) varies from 2 to 10 kW m^{-2}. The compressor capacity is progressively varied from 30 % to 100 % at constant water flow rate in a first data set, and at constant inlet water temperature (12 °C) in a second one, running experimental tests in the Onda Heat Transfer Laboratory. The maximum heat fluxes obtained for the two different fluids differ each other reflecting the same difference in the volumetric capacity, being 25 % lower for R1234ze(E) than for R134a. Considering the evaporator, at a given capacity the value of the water-to-saturation temperature approach for R1234ze(E) results very similar to that of R134a.
The experimental data are compared to the results of a software simulation developed specifically for the evaporator. The critical parameters for the model are the characteristics of the new HFO fluid and the low mass fluxes. Specific literature models were chosen for the water heat transfer coefficient, for the superheated vapor heat transfer coefficient and pressure drop (concentrated and distributed), for the dry-out inception quality, for the two-phase concentrated and distributed pressure drop. The evaporating heat transfer coefficient, instead, was calculated with two different literature models, respectively Cavallini *et al.* (2006) and Mehendale (2018). For both the models used, the simulation results are in good agreement with the experimental data.

1. INTRODUCTION

Warming in the earth climate system is unprecedented over decades to millennia, and greenhouse gas emissions caused by human activity plays an important role on it (Stocker *et al.*, 2013). In Europe, Regulation (EU) No. 517/2014 on fluorinated greenhouse gases (F-gases) has introduced a roadmap towards move to a competitive low carbon economy in 2050, and it specifies a range of progressive steps to define the HFC phase-down (European Parliament, 2014).
In this regard, a primary challenge is the substitution of the fluid R134a. A choice already quite established is the fluid R1234ze(E), a hydrofluoro-olefin (HFO). From the environmental point of view it is far better than R134a, not only in terms of GWP (less than 1, versus 1430), but also in terms of its atmospheric lifetime (about 2 weeks, compared to 13 years) (Hodnebrog *et al.*, 2013). Its atmospheric oxidation products, moreover, have negligible

environmental impact (Javadi *et al.*, 2008). Anyway, it carries two main disadvantages: a slight flammability, and a vapor compression process generally less performing than that of R134a.
In case of a direct drop-in replacement of R134a with R1234ze(E) in an existing plant, using a positive displacement compressor according to a basic vapor compression cycle (VCC), at the same saturation temperatures the coefficient of performance (*COP*) is almost equal. However, the maximum cooling capacity is significantly reduced (about -25 %, or less), due to the lower volumetric capacity of R1234ze(E) as compared to R134a. A recent related detailed theoretical study on the efficiency of this and other low-GWP fluids can be found in McLinden *et al.* (2017).
The work of Sánchez *et al.* (2017) reports an experimental confirmation of the reduced efficiency of the compressor. In a VCC machine with brazed plate type condenser and evaporator, previously tested with R134a, at the same condensing and evaporating temperatures the fluid R1234ze(E) yields a reduction of the cooling capacity of 24.9 %.
An experimental analysis of a whole evaporator, directly comparing R134a and R1234ze, is described by Righetti *et al.* (2014), regarding a roll-bond heat exchanger for a small size domestic refrigerator. The evaporating temperatures were -15 C° and -20 °C, the mass fluxes ranged from 10 to 60 kg $m^{-2}s^{-1}$, with maximum cooling capacity 100 W. They found the same heat transfer performances in the roll-bond evaporator for both fluids, and the data were well predicted by a pool boiling correlation. They explain it with the low values of the mass fluxes (like the ones in the present work), which imply very low values of the liquid Reynolds number and consequently a poor effect of the convective boiling contribution, leaving the pool boiling as the prevailing heat transfer mechanism.
As an example of a study of the heat transfer capabilities of R1234ze(E) during two-phase flow inside a single enhanced tube, Kedzierski and Park (2013) experimentally investigated the evaporation of R134a and R1234ze(E) inside a microfin tube with inner diameter 8.92 mm. At the same constant heat and mass flux, and the same constant evaporating temperature, the local heat transfer of R1234ze(E) was always lower than that of R134a ($G > 100$ kg $m^{-2}s^{-1}$). The gap is primarily addressed to the smaller thermal conductivity and the smaller reduced pressure of R134ze(E).
Diani *et al.* (2014) measured the heat transfer coefficients of R134a and R1234ze(E) evaporating in a 3.4 mm ID microfin tube ($190 < G < 940$ kg $m^{-2}s^{-1}$). The heat transfer coefficient almost always increased with vapor quality, mass flux, and heat flux, before the inception of the dryout. The heat transfer coefficients measured for R1234ze(E) were at least around 8 - 10% lower than the ones obtained for R134a, and the measured pressure gradient of R1234ze(E) always surpassed the one of R134a.
The present work aims directly to compare the performance of R134a and R1234ze(E) in a whole, industrial purposed shell-and-tube dry-expansion (DX) microfin tube evaporator. The working conditions are set to the typical air conditioning values, and all the measured values of the cooling capacity are less than 250 kW. A similar comparison, but between R134a and R1234yf, is reported by Mendoza-Miranda *et al.* (2015).

2. DESIGN OF THE PROTOTYPE

The evaporator considered is a shell-and-tube heat exchanger using micro-fin copper tubes with outer diameter equal to 7.94 mm. The water to be chilled flows on the shell side, with a forced local cross-flow motion induced by single-segmental baffles. The sketch in Figure 1 reflects the overall geometry of the evaporator, with a shell diameter equal to 0.273 m and tube length 2.6 m.
The refrigerant evaporates inside the tubes, and on the inlet header a local refrigerant pressure drop is generated by a distribution device, whose characteristics are the same described by Del Col *et al.* (2015). In order to achieve an outlet refrigerant superheating approximately equal to 5 K and a water-to-saturation approach at least equal to 2 K, the overall configuration of the two fluids is countercurrent (although locally, as already mentioned, the flows cross each other).

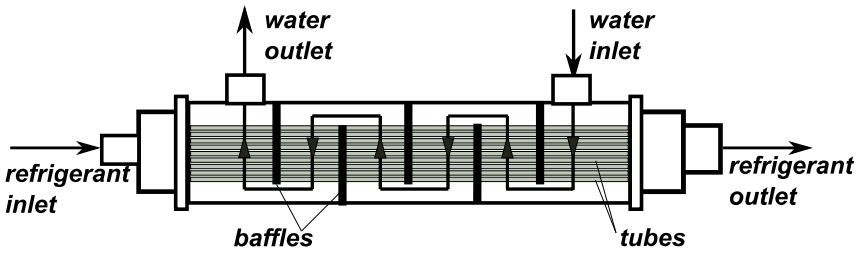

Figure 1: Qualitative description of the heat exchanger considered.

3. EXPERIMENTAL STUDY OF THE EVAPORATOR

3.1 Experimental test rig

The experimental tests were conducted on the apparatus set up at the laboratory of Onda S.p.A., Italy, schematic of which is depicted in Figure 2. For the tests, the system was charged with R134a first, and then with R1234ze(E); between the two operations, the plant was cleaned with nitrogen.

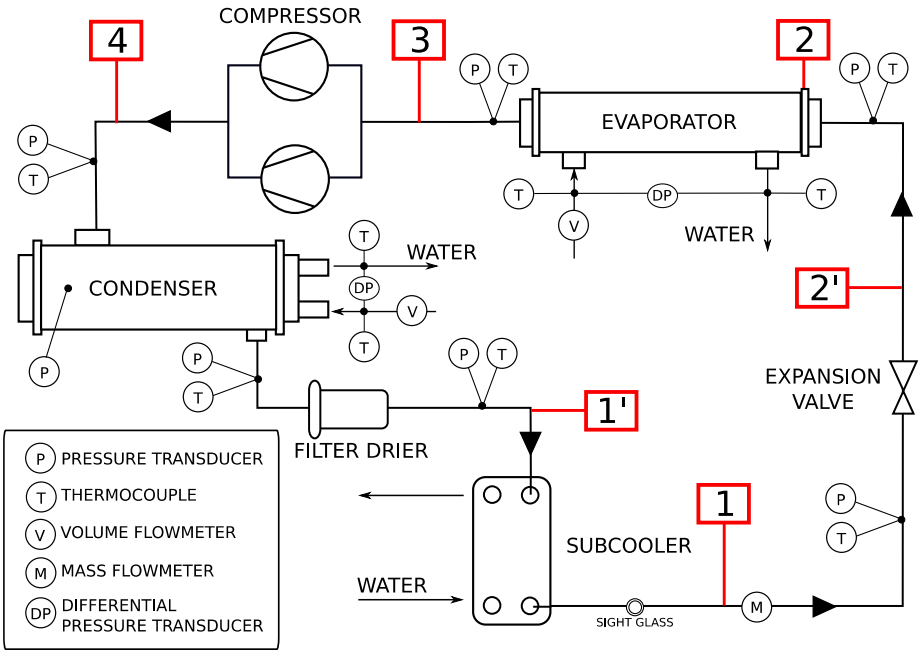

Figure 2. Test apparatus (1-2: lamination; 2-3: evaporation; 3-4: compression; 4-1: desuperheating, condensation, and subcooling)

The tests are conducted varying the compressor capacity from 100 % to 30 %; the lubricant used has kinematic viscosity at 40 °C equal to 32 cSt, and its concentration in the circuit is estimated to amount to less than 3 %.
The compressed hot vapor refrigerant is saturated, condensed and subcooled in a shell-and-tube heat exchanger (the condenser), where the condensing temperature can be varied in a short range by modulating the water flow rate. The liquid refrigerant at the condenser exit is additionally subcooled in a brazed plate heat exchanger, where the water enters at the same temperature as in the evaporator, and the value of its flow rate determines the subcooling degree needed to reach the required vapor quality at the evaporator inlet. The expansion device is a step motor electronic valve, whose opening is varied manually according to the required superheating at the evaporator exit.

Table 1: Accuracy for sensors and parameters (at typical test conditions).

Parameter	**Accuracy**
Temperature	±0.05 K
Water volumetric flow rate	±0.5 %
Refrigerant mass flow rate	±0.5 %
Absolute pressure	±1 kPa
Differential pressure	±200 Pa
Temperature difference	±0.10 K
Temperature approach	±0.12 K
Heat flux	±3 %
Global heat transfer coefficient	±5 %

3.2 Measure system, operative conditions and data reduction

The water temperatures at the inlet and outlet of the heat exchangers are measured by thermocouples inserted in adiabatic sections, where perfect mixing is assured. Type J thermocouples connected to a Kaye ice point instrument as zero reference system are used; they were calibrated on site using a primary Pt100 probe and a reference bath to get the accuracy value reported in Table 1.

The water volume flow rates and pressure drops through the heat exchangers are measured with electromagnetic flow meters and differential pressure transducers, respectively. Finally, a Coriolis effect flow meter measures directly the refrigerant mass flow rate. In this way, the thermal balances between water and refrigerant side are checked. The values of the mass velocity range from 30 to 100 kg m^{-1} s^{-2} for R134a, and from 26 to 80 kg m^{-1} s^{-2} for R1234ze(E).

For each refrigerant, two different sets of tests are considered: one with constant inlet and outlet water temperatures, and one with constant water outlet temperature and flow rate, maintaining the evaporator tube inlet vapor quality and the outlet superheating constant.

The tube inlet vapor quality is obtained from the enthalpy of the refrigerant at the evaporator inlet, considered equal to the liquid enthalpy obtained measuring the liquid temperature and pressure before the expansion valve. Its value is kept at 0.25 kg/kg.

The value of the reference evaporating temperature $t_{sat,3}$ is obtained from the pressure p_3 measured at the evaporator exit, and combined with the measured temperature t_3 it allows to get the value of the superheating. From p_3 and t_3 the outlet enthalpy, and finally the heat flow rate on the refrigerant side, are also calculated.

On the water side, instead, the heat flow rate is obtained from the measured values of the temperatures and of the volume flow rate. Tests with differences between water and refrigerant capacities higher than 5 % are not validated; the average deviation is found to be about 3 %.

The average heat flux at the evaporator ranges from 2.9 to 9.4 kW m^{-2} for R134a, and from 2.2 to 7.2 kW m^{-2} for R1234ze(E) (both from 30 % to 100 % of the maximum available capacity). The local heat flux, instead, is estimated based on the heat transfer models used: the approximate range is from 1 to 32 kW m^{-2} for R134a, and from 0.5 to 25 kW m^{-2} for R1234ze(E). The value of average heat flux is linked to the water-to-saturation temperature approach at the evaporator outlet pipe ($\Delta t_{app} = t_{W,lea} - t_{sat,3}$), which, lower its value, higher the suction pressure, the capacity given by the compressor and the machine COP. The measured values of Δt_{app} range from 1.1 to 4.1 K.

All the thermophysical properties of R134a, R1234ze(E) and water are calculated by means of the Refprop 10.0 software (Lemmon *et al.*, 2018).

3.3 Experimental results

A direct comparison between the two fluids at the condition Δt_W = 5 K (in particular, water entering at about 12 °C and leaving at about 7 °C) is illustrated in Figure 3a). Figure 3b), instead, compares the two fluids at a water flow rate 9.5 kg s^{-1}; this value corresponds to the optimal water parameters for which the evaporator was designed, namely cross-flow velocity and pressure drop.

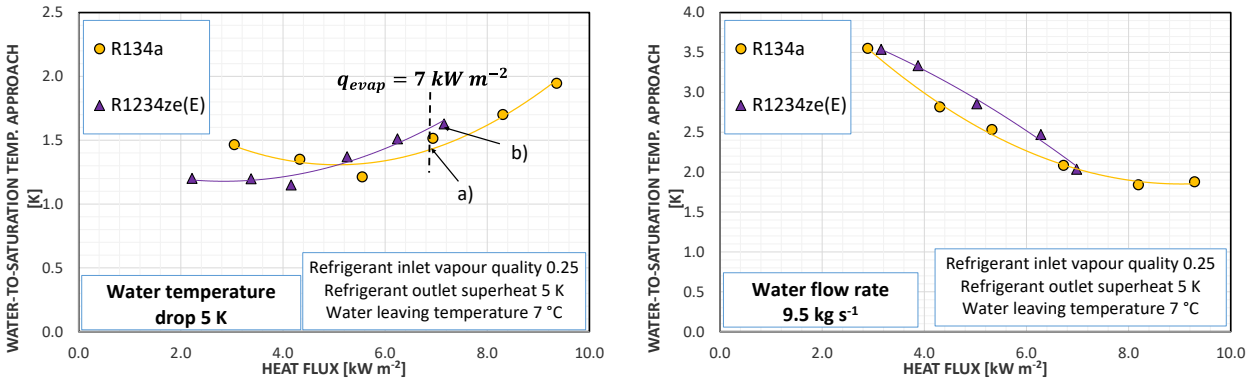

a) b)

Figure 3: Comparison of the experimental water-to-saturation temperature approach at the outlet of the evaporator, plotted versus the heat flux, for R134a and R1234ze(E). a) Constant water temperature drop; b) Constant water flow rate.

The maximum heat fluxes obtained for the two different fluids (9.4 kW m^{-2} for R134a and 7.2 kW m^{-2} for R1234ze(E)) differ each other reflecting the same difference between the predicted values of the volumetric capacity, which for R134ze(E) is 25 % lower than for R134a.
Starting from 100 % capacity, the curves with Δt_W = 5 K show that the water-to-saturation approach decreases as the capacity decreases until seemingly reaching a minimum, then it tends to stop and to reverse the trend. This minimum is evident with R134a just below 50 % of the maximum capacity, whereas for R1234ze(E), although not observed, it is expected to occur for around 30 % of the maximum capacity.
Such behavior can be explained considering that, being constant the water temperatures, the water-to-saturation approach has an identical trend, and an identical dependance on q, of the logarithmic temperature difference Δt_{ln}. Temporarily neglecting the superheating, it is:

$$\Delta t_{ln} = \frac{q}{K} \tag{1}$$

and considering that K is a function of q too, the first order derivative gives:

$$\frac{d(\Delta t_{ln})}{dq} = \frac{1}{K} - \frac{q}{K^2}\frac{dK}{dq} \tag{2}$$

An increase of q gives an increase of the water and refrigerant flowrate, and an increase of their relative heat transfer coefficients: then the global heat transfer coefficient K increase too, and $dK/dq > 0$ always. If q_{min} is the value of the heat flux where that minimum occurs, for $q = q_{min}$ a given variation of the heat flux is perfectly balanced by the corresponding variation of the global heat transfer coefficient. Then no change on Δt_{ln} (and on the water-to-saturation approach) is required ($d(\Delta t_{ln})/dq = 0$), and Equation (2) indicates $dK/dq = K/q$. Observing Figure 3a), moreover, for $q > q_{min}$ it is $d(\Delta t_{ln})/dq > 0$: Δt_{ln} must increase because K does not vary strongly with q ($dK/dq < K/q$). For $q < q_{min}$, instead, an imposed increase of the heat flux implies a very high increase of the global heat transfer coefficient ($dK/dq > K/q$), and Δt_{ln} decreases to compensate it ($d(\Delta t_{ln})/dq < 0$).
A completely different behavior is expressed by the curves with constant water flow rate, showing an increase of the approach (whose behavior is in general different, now, from that of Δt_{ln}) as the capacity decreases. In general, it is a trend opposite to what it is commonly observed for the classical evaporators with high values of the water-to-saturation approaches.
In the present case the approach is low, and the entering water temperature, at constant water flow rate and constant leaving temperature, decreases as the capacity decreases. The requirement of 5 K superheat, then, "pushes" the saturation temperature to values lower than the initial one. For such conditions, the water side heat transfer coefficient is constant, and an increase of the capacity is partly due to an increase of K, to which only the refrigerant contributes, and partly to an increase of the mean logarithmic temperature difference Δt_{ln}.
In Figure 3a), the curves cross each other at around 5 kW m^{-2}; over this value of the heat flux the R134a performance results slightly better than the one of R1234ze(E). Points a) and b) in Figure 3a) can be taken as an example: they are taken at almost the same heat flux (7 kW m^{-2}), and the approaches differ only slightly. As the capacity is the same, the water flow rates and its heat transfer coefficients are the same for both points; the performance differences can be ascribed only to the refrigerant, whose heat transfer coefficient is composed essentially by a nucleate boiling and a convective boiling component.
At the above conditions, the reduced pressure of R1234ze(E) is 17 % lower than that of R134a and the molar mass is 12 % higher: both occurrences penalize the nucleate boiling component. The convective boiling component, instead, is in general connected to the liquid heat transfer coefficient, and the lower value of the liquid thermal conductivity of R1234ze(E) (-10 %) penalizes it. Anyway, the flow rate of R1234ze(E) is higher, as the heat of vaporization is lower, and the capacity is the same: also its liquid Reynolds number is higher and it improves the convective boiling performance.
The heat transfer performance, expressed in terms of the water-to-saturation temperature approach, is affected also by the refrigerant pressure drop along the tubes. At the same outlet pressure, high pressure drops generate low logarithmic temperature differences, and then, at the same conditions, low capacities. The present tests do not contemplate measurements of the tube pressure drop, but of the total pressure drop of the refrigerant trough the evaporator: the part due to the inlet distribution device is included in the measure (Figure 4). According to estimations of in-tube pressure drop, the concentrated pressure drop is sharply dominant. At the same mass velocity, the pressure drop measured for R1234ze(E) results around 15 - 20 % higher than the one for R134a. But, if we consider two test points at the same capacity, the difference between the pressure drop of the two fluids is

consistently higher. For example, coming back to the points a) and b) in Figure 3a), the mass velocity of R1234ze(E) is +10 % higher. The total effect is a refrigerant pressure drop 40 % higher. Moreover, for R1234ze(E) the value of $(dt/dp)_{sat}$ calculated with Refprop 10.0 (Lemmon *et al.*, 2018), at the given conditions, is another 33 % more. In total, then, it is predicted to have a total saturation temperature drop of R1234ze(E) 86 % higher than the one of R134a. Only the part distributed along the tubes, anyway, contributes to the reduction of the logarithmic temperature difference.

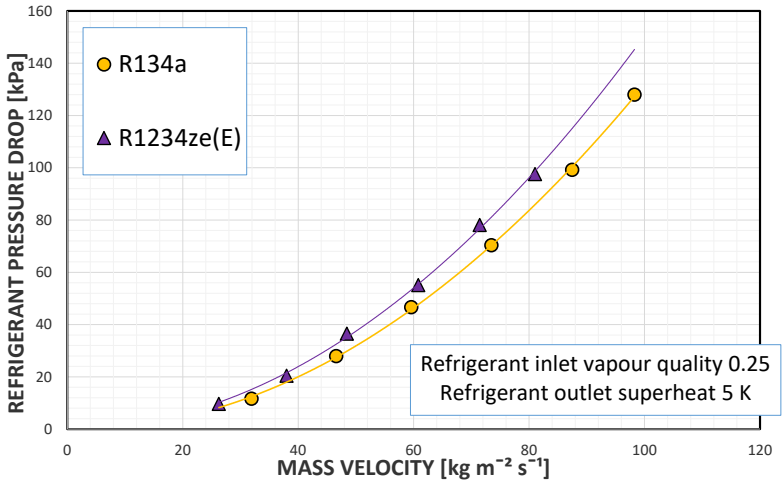

Figure 4: Comparison of the experimental refrigerant pressure drop trough the evaporator, plotted versus the mass velocity, for R134a and R1234ze(E).

4. PREDICTIVE STUDY OF THE EVAPORATOR

4.1 Predictive algorithm, heat transfer and pressure drop models

The geometric and flow configurations of the heat exchanger are relatively simple, being a shell-and-tube heat exchanger with two fluids in an almost counter-current arrangement. This background suggests a calculation by means of a simplified method with averaged parameters. However, the evolution of the state of refrigerant is quite complex. It starts as a two-phase mixture, meeting a discontinuity on the rate of variation of many thermodynamical parameters when the dry-out takes place at high values of the vapor quality, and it exits the heat exchanger as single-phase vapor. Thus, a local calculation procedure, fully physically consistent, is here preferred. The method presented is based on the basic thermal design equation:

$$dA = \frac{dQ}{K(t_W - t_R)} \tag{3}$$

with the scope, as explained by Bell (2004), to formally integrate it and find the heat transfer area:

$$A_{evap} = \int_{Q=0}^{Q=Q_{evap}} \frac{dQ}{K(t_W - t_R)} \tag{4}$$

Table 2 reports the models used for the calculation procedure, all taken from the open literature with one exception, the concentrated pressure drop trough the inlet distribution device. That parameter, in fact, is calculated by means of an empirical correlation obtained by present authors from their own previous experimental data on the same evaporator.

The integration is possible as t_W and t_R, the local temperatures of the water and refrigerant, respectively, are both functions of the quantity of heat that has been transferred from the beginning of the calculation. Moreover, the local overall heat transfer coefficient K is also indirectly a function of the heat transferred, as local flow conditions and thermal properties change with the temperatures.

The integration (numerical) is performed applying a finite difference method, starting from the refrigerant outlet and proceeding backwards with respect to the refrigerant flow. As shown in Figure 5, three different heat transfer zones are considered, with in addition two adiabatic parts at the inlet and at the outlet respectively; the number assigned to each part reflects the respective order of calculation. In sequence, they are: first, the refrigerant adiabatic single-phase flow (superheated vapor) at the outlet header (part 0); then, the refrigerant diabatic single-phase flow (superheated vapor) inside the tubes (part 1); then, the refrigerant evaporating two-phase flow after the dry-out (part 2); then, the refrigerant evaporating two-phase flow with wet walls, before the dry-out (part 3); finally, the refrigerant adiabatic two-phase flow at the inlet header (part 4).

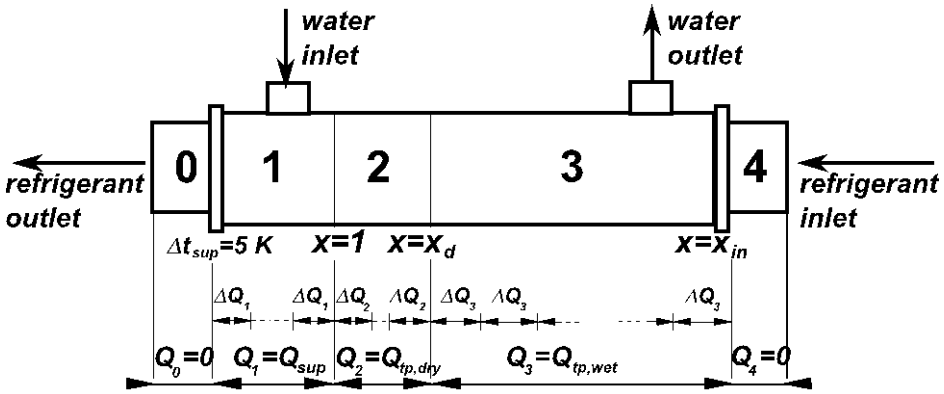

Figure 5: Schematization of the evaporator as arranged for the calculation.

Table 2: Heat transfer, pressure drop and dry-out quality models used for the calculation procedure.

Fluid	Evaporator part	Parameter	Model
Water	All	Pressure drop	Bell (1960)
		Heat transfer coefficient	
Refrigerant	Superheated vapor	Concentrated pressure drop	Henry (1992)
		Distributed pressure drop	Jensen and Vlakancic (1999)
		Heat transfer coefficient	
	Two-phase flow	Dry-out inception vapor quality	Padovan *et al.* (2011)
		Concentrated pressure drop	Paliwoda (1992) and present authors' empirical correlation
		Distributed pressure drop	Cavallini *et al.* (1997)
	Two-phase flow after dry-out	Heat transfer coefficient	Linear interpolation
	Two-phase flow before dry-out	Heat transfer coefficient	Cavallini *et al.* (2006)
			Mehendale (2018)

The procedure is used in order to obtain either the refrigerant leaving pressure $p_{R,lea}$ or the heat capacity Q_{evap}: one of them is supposed known and simply imposed equal to the experimental measure. The value of other one, which is chosen as the final output of the calculation and considered unknown, is guessed and used to calculate the heat transfer surface area according to Equation (4). If this area differs from the real heat transfer area more than a pre-fixed tolerance (namely 0.5 %), the unknown parameter is modified until reaching convergence. In particular, if $A_{evap,calc}$ results higher than $A_{evap,real}$, a lower value of the unknown parameter ($p_{R,lea}$ or Q_{evap}) is re-guessed, and vice-versa.

The refrigerant flow boiling heat transfer (before dry-out) is the most influential parameter that determines the output of the calculation, and two heat transfer coefficient models are taken into consideration in this work: Cavallini *et al.* (2006) and Mehendale (2018).

The structure of the Cavallini *et al.* (2006) method is additive: the flow boiling heat transfer coefficient results as the sum of three terms, due respectively to the nucleate boiling, to the forced convection, and to the capillarity action in

the micro grooves. The Mehendale (2018) model, instead, is multiplicative: the two-phase Nusselt number is obtained as the product of some dimensionless parameters, previously identified as the most influential to the heat transfer process, with empirical exponents obtained by a best-fitting procedure.
It is worth noting that, whereas the model by Mehendale (2018) was developed by its author considering also R1234ze(E) data, the model by Cavallini *et al.* (2006) did not include for its realization any HFO experimental data. Both models, instead, include R134a data.

4.2 Comparison between calculated and experimental data

Figure 6 presents the results of the application of the predictive algorithm. Every simulation is run first imposing the exchanged heat flow rate and calculating the evaporation temperature (Figure 6a), second imposing the evaporation temperature and calculating the exchanged heat flow rate (Figure 6b).

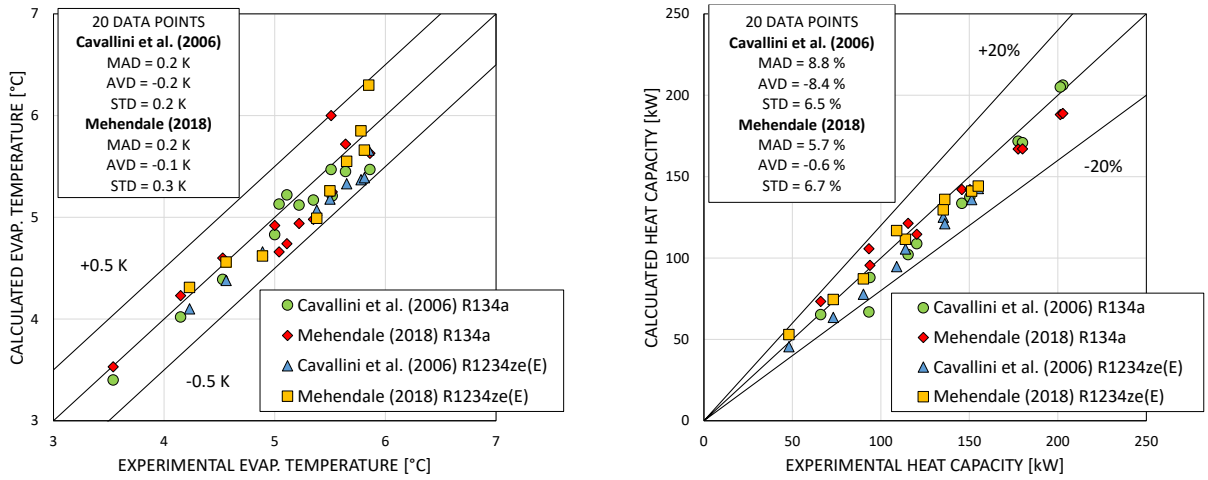

a) b)

Figure 6: Experimental data compared to the results of the simulations with different flow boiling heat transfer coefficient models and different fluids: a) evaporation temperatures at the experimental heat flow rates; a) heat flow rates at the experimental evaporation temperatures.

Figure 6 reports the statistical parameters resulting from the comparison between the experimental and the calculated data, for each model respectively. Let y be the chosen parameter, either the evaporation temperature ($y=t_{sat}$) or the relative heat flow rate ($y=Q/Q_{EXP}$); the single point deviation is defined as:

$$\Delta y = y_{CALC} - y_{EXP} \tag{5}$$

The set of the N data compared is the sample considered. The parameters reported in Figure 6 are the mean absolute deviation (*MAD*), the average deviation (*AVD*), and the standard deviation (*STD*), defined respectively as:

$$MAD = \frac{1}{N}\sum_{i=1}^{N}|\Delta y| \tag{6}$$

$$AVD = \frac{1}{N}\sum_{i=1}^{N}\Delta y \tag{7}$$

$$STD = \sqrt{\frac{\sum_{i=1}^{N}(\Delta y - AVD)^2}{N-1}} \tag{8}$$

Regarding the prediction of the evaporation temperature, there are no significant differences between the two models (both giving a mean absolute deviation of 0.2 K). A slight difference is instead found on the prediction of the heat capacity, with a mean absolute deviation of 8.8 % for the model by Cavallini *et al.* (2006) and of 5.7 % for the model by Mehendale (2018).

5. CONCLUSIONS

The tests and the predictive simulations performed comparing the behavior of R134a and R1234ze(E) in a shell-and-tube evaporator inserted in a vapor compression cycle lead to the following conclusions:

- The maximum heat capacity obtained for R1234ze(E) is 25 % lower than for R134a, reflecting the same difference in the volumetric capacity at the same cycle conditions.
- For both fluids, when reducing the heat flux, the value of the water-to-saturation temperature approach increases at constant water flow rate, whereas it decreases at variable water flow rate.
- At a given heat flux, the value of the overall heat transfer coefficient for R1234ze(E) results very similar to that of R134a: it means that the same evaporator gives similar performances.
- The simulation of the whole heat exchanger by means of a finite differences method gives results strongly influenced by the model used for the evaporation heat transfer coefficient.
- The comparison of the experimental data with the results of the calculations done by the application of two different literature models for the evaporation heat transfer coefficient denotes a good agreement for both fluids.
- In particular, the Cavallini *et al.* (2006) model, and the more recent one by Mehendale (2018), obtained from databanks respectively without and with R1234ze(E), leads to very similar results of the predictions.

NOMENCLATURE

A	heat transfer surface area	(m^2)
AVD	average deviation	
dt/dp	derivative of the temperature as a function of the pressure	(K Pa^{-1})
G	mass flux, or mass velocity	(kg m^{-2} s^{-1})
K	overall heat transfer coefficient	(W m^{-2} K^{-1})
MAD	mean absolute deviation	
N	sample size	
p	pressure	(Pa)
q	heat flux	(W m^{-2})
Q	heat flow rate	(W)
STD	standard deviation	
t	temperature	(K)
x	vapor quality	(kg kg^{-1})
Δt	temperature difference	(K)

Subscript

app	approach
calc	calculated
evap	evaporator
lea	leaving
ln	mean logarithmic
min	minimum
R	refrigerant
real	real
sat	saturated
sup	superheated
W	water

REFERENCES

Bell, K. J. (1960, October). Exchanger Design… based on the Delaware Research Program. *Petro/Chem Engineer*, p. C26-40c.

Bell, K. J. (2004). Heat Exchanger Design for the Process Industries. *Journal of Heat Transfer, 126*(6), p. 877–85.

Cavallini, A., Del Col, D., Doretti, L., Longo, G. A., & Rossetto, L. (1997). Pressure drop during condensation and vaporisation of refrigerants inside enhanced tubes. *International Journal of Heat and Technology, 15*(1), p. 3-10.

Cavallini, A., Del Col, D., & Rossetto, L. (2006). Flow boiling inside microfin tubes: prediction of the heat transfer coefficient. . *ECI International Conference on Boiling Heat Transfer.* Spoleto, Italy.

Del Col, D., Bortolin, S., Censi, G., & Da Riva, E. (2015). Impact of two-phase distribution systems on the performance of a microchannel evaporator. *Science and Technology for the Built Environment, 21*(7), p. 1047-58.

Diani, A., Mancin, S., & Rossetto, L. (2014). R1234ze(E) flow boiling inside a 3.4 mm ID microfin tube. *International Journal of Refrigeration, 47*, p. 105-19.

European Parliament. (2014). Regulation (EU) No 517/2014 of the European Parliament and of the Council of 16 April 2014 on fluorinated greenhouse gases and repealing Regulation (EC) No 842/2006. *Official Journal of the European Union*.

Henry, J. (1992). Single-phase flow. Headers, nozzles, and turnarounds. In G. F. Hewitt, *Handbook of Heat Exchanger Design* (p. 2.2.7.1-11). New York, NY, USA and Wallingford, United Kingdom: Begell House, Inc.

Hodnebrog, Ø., Etminan, M., Fuglestvedt, J. S., Marston, G., Myhre, G., Nielsen, C. J., Shine, K. P., & Wallington, T. J. (2013). Global Warming Potentials and Radiative Efficiencies of Halocarbons and Related Compounds: A Comprehensive Review. *Reviews of Geophysics, 51*(2), p. 300-78.

Javadi, M. S., Søndergaard, R., Nielsen, O. J., Hurley, M. D., & Wallington, T. J. (2008). Atmospheric chemistry of trans-CF3CH=CHF: products and mechanisms of hydroxyl radical and chlorine atom initiated oxidation. *Atmospheric Chemistry and Physics, 8*, p. 1069-88.

Jensen, M. K., & Vlakancic, A. (1999). Technical Note. Experimental investigation of turbulent heat transfer and fluid flow in internally finned tubes. *International Journal of Heat and Mass Transfer, 42*(7), p. 1343-1351.

Kedzierski, M. A., & Park, K. J. (2013). *Horizontal Convective Boiling of R134a, R1234yf/R134a, and R1234ze(E) within a Micro-Fin Tube with Extensive Measurement and Analysis Details.* Technical Note 1807, National Institute of Standards and Technology.

Lemmon, E. W., Bell, I. H., Huber, M. L., & McLinden, M. O. (2018). NIST Standard Reference Database 23: Reference Fluid Thermodynamic and Transport Properties-REFPROP, Version 10.0. *Standard Reference Data Program*. Gaithersburg, USA.

McLinden, M. O., Brown, J. S., Brignoli, R., Kazakov, A. F., & Domanski, P. A. (2017). Limited options for low-global-warming-potential refrigerants. *Nature Communications, 8*, p. 14476.

Mehendale, S. (2018). A new heat transfer coefficient correlation for pure refrigerants and near-azeotropic refrigerant mixtures flow boiling within horizontal microfin tubes. *International Journal of Refrigeration, 86*, p. 292-311.

Mendoza-Miranda, J. M., Ramírez-Minguela, J. J., Muñoz-Carpio, V. D., & Navarro-Esbrí, J. (2015). Development and validation of a micro-fin tubes evaporator model using R134a and R1234yf as working fluids. *International Journal of Refrigeration, 50*, p. 32-43.

Padovan, A., Del Col, D., & Rossetto, L. (2011). Experimental study on flow boiling of R134a and R410A in a horizontal microfin tube at high saturation temperature. *Applied Thermal Engineering, 31*, p. 3814-26.

Paliwoda, A. (1992). Generalized method of pressure drop calculation across pipe components containing two-phase flow of refrigerants. *International Journal of Refrigeration, 15*(2), p. 119-25.

Righetti, G., Zilio, C., & Longo, G. A. (2014). Experimental Analysis of R134a and R1234ze(E) Flow Boiling Inside a Roll Bond Evaporator. *International Refrigeration and Air Conditioning Conference at Purdue.* West Lafayette, Indiana, USA.

Sánchez, D., Cabello, R., Llopis, R., Arauzo, I., Catalán-Gil, J., & Torrella, E. (2017). Energy performance evaluation of R1234yf, R1234ze(E), R600a, R290 and R152a as low-GWP R134a alternatives. *International Journal of Refrigeration, 74*, p. 269-82.

Stocker, T. F., Qin, D., Plattner, G.-K., Tignor, M. M., Allen, S. K., Boschung, J., Nauels, A., Xia, Y., Bex, V., & Midgley, P. M. (2013). *IPCC, 2013: Climate Change 2013: The Physical Science Basis. Contribution of Working Group I to the Fifth Assessment Report of the Intergovernmental Panel on Climate Change.* Cambridge, United Kingdom and New York, NY, USA: Cambridge University Press.